RDA-TR-126600-001

APRIL 1986

AFOSR-TR- 88-0098

[redacted] FINAL REPORT

UNIFIED STUDY OF PLASMA-SURFACE INTERACTIONS FOR SPACE POWER AND PROPULSION

Submitted to:

Directorate of Aerospace Sciences
Air Force Office of Scientific Research
Bolling Air Force Base
Washington, DC 20332

Prepared by:

RDA/WRL Staff

TABLE OF CONTENTS

SECURITY CLASSIFICATION OF THIS PAGE (When Data Entered)

REPORT DOCUMENTATION PAGE		READ INSTRUCTIONS BEFORE COMPLETING FORM
1. REPORT NUMBER AFOSR-TR- 88-0098	2. GOVT ACCESSION NO.	3. RECIPIENT'S CATALOG NUMBER
4. TITLE (and Subtitle) Unified Study of Plasma-Surface Interactions for Space Power and Propulsion		5. TYPE OF REPORT & PERIOD COVERED FINAL 1 May '83-31 Aug '84
		6. PERFORMING ORG. REPORT NUMBER RDA-TR-126600-001
7. AUTHOR(s) RDA/WRL Staff		8. CONTRACT OR GRANT NUMBER(s) F49-620-83-C-0105
9. PERFORMING ORGANIZATION NAME AND ADDRESS R & D Associates Washington Research Laboratory 301 S West St., Alexandria, VA 22314		10. PROGRAM ELEMENT, PROJECT, TASK AREA & WORK UNIT NUMBERS 61102F 2308/K1
11. CONTROLLING OFFICE NAME AND ADDRESS Air Force Office of Scientific Research Bldg. 410, Bolling Air Force Base Washington, DC 20332 NA		12. REPORT DATE April 1986
		13. NUMBER OF PAGES 35
14. MONITORING AGENCY NAME & ADDRESS(if different from Controlling Office) Same as 11		15. SECURITY CLASS. (of this report) Unclassified
		15a. DECLASSIFICATION/DOWNGRADING SCHEDULE
16. DISTRIBUTION STATEMENT (of this Report) ~~AFOSR Directorate of Aerospace Sciences~~		
17. DISTRIBUTION STATEMENT (of the abstract entered in Block 20, if different from Report) n/a		
18. SUPPLEMENTARY NOTES n/a		
19. KEY WORDS (Continue on reverse side if necessary and identify by block number) plasma; surfaces; magnetogasdynamics; electric propulsion		

20. ABSTRACT (Continue on reverse side if necessary and identify by block number)

The overall aim of the present three-year research program is the study of interaction between plasmas, whose parameters are typical of high specific power, high specific impulse devices, and various conducting and insulating surfaces. This study is carried out using metallic and dielectric surfaces arranged perpendicular (facing upstream and downstream) and parallel to the plasma stream supplied by a quasi-steady

DD FORM 1 JAN 73 1473 EDITION OF 1 NOV 65 IS OBSOLETE

SECURITY CLASSIFICATION OF THIS PAGE (When Data Entered)

I. ABSTRACT

The overall aim of the present three-year research program is the study of interaction between plasmas, whose parameters are typical of high specific power, high specific impulse devices, and various conducting and insulating surfaces. This study is carried out using metallic and dielectric surfaces arranged perpendicular (facing upstream and downstream) and parallel to the plasma stream supplied by a quasi-steady MPD arcjet. These phenomena, when they have been investigated at all, have been studied under the parameter constraints of particular devices, usually under conditions of poor diagnostic accessibility. The present study is carried out under conditions that allow better diagnostic examination of the plasma-surface region with the ability to vary plasma parameters, flow relative to the samples, electrical conduction to the (metal) samples, etc. The aim is to delineate the basic physics of plasma-surface interaction under conditions applicable to the design of space power and propulsion systems.

In the first phase of this work the basic experimental apparatus has been assembled and tested. This includes a 0.6 by 6 m cylindrical vacuum tank and a 20 kJ pulse forming network capable of supplying a 150 μs pulse. Preliminary tests have been carried out in the system using a plasma railgun that produces plasmas with temperatures of about 7 eV and flow velocities of the order of 2 cm/μs. Spectroscopic, refractive, and probe measurements have been made of the flow from the gun and in the space between the electrodes. The MPD arcjet has been built and is ready for installation in the system.

In the early part of the second phase of the work, the arcjet will be installed and tested; the downstream plasma flow will be examined and its parameters (temperature, composition, density, flow velocity, etc.) will be correlated with the variation in the discharge energy and other parameters of the thruster. This work may also be extended to the plasma in and

near the thruster, thus providing information about the mechanisms of the MPD arcjet itself. In the major portion of this second phase, we shall introduce the surface samples and undertake the systematic study of interactions with the plasma flow.

II. INTRODUCTION

The number of defense-related systems in space and their level of sophistication has increased greatly over the past two decades since such systems first became practical. It is relatively certain that the number and mass of such systems will continue to increase over the foreseeable future. This being the case, a rapid improvement in our prime space power and thruster technology is called for in order to make such defense systems practical from a technological and economic point of view. As history has shown with sea and air power, those craft that can be deployed further and remain on station longer with high system capability can control larger portions of their medium, whether ocean, air, or space.

For rocket thrusters, whether chemical or electric, the change in the velocity of the spacecraft is proportional to the logarithm of the ratio of initial to final mass. The constant of proportionality is the exhaust velocity of the thruster. Since logarithms vary quite slowly as a function of their arguments and low fuel mass is, in any case, desirable, clearly it behooves us to consider thrusters capable of quite high exhaust velocities. Further consideration of the problem in terms of specific power (defined as the power available to the thruster divided by the spacecraft mass less the fuel mass) shows that under optimal conditions the specific power and exhaust velocity are functionally related ($P_{sp} \propto u^2_{exh}/\tau$) where τ is the mission length or burn-out time. The highest exhaust velocities are thus practical only when high specific power is also available, or when long mission times are contemplated. At projected levels of specific power, the particle energies in the thruster will be in the range of 10-50 eV, with plasma temperatures of a few electron volts.

Electromagnetic thrusters are analogous to motors where the working fluid plays the role of the armature. As is the case with motors, the flow of energy can be reversed so that the device can also act as an electrical power source or generator. In either case, solid surfaces must be used to channel the

working fluid which will be a plasma with temperatures in the range of 0.5-10 eV and directed energies per ion in the range of 0.5-100 eV. Whether or not this desirable range of particle energies can be employed in a reliable flight-worthy system depends critically on the behavior of dielectric (e.g., teflon, nylon, boron nitride) and metal (e.g., copper, brass, tungsten) surfaces in intimate contact with the plasma environment. A practical laboratory assessment of such behavior depends on a knowledge of the physical mechanisms at work in the interaction. This is not just a question of measuring damage rate; the electrode sheath details determine the voltage falls which critically affect specific power and can also play a decisive role in waste heat production and erosion rate. Thus, in order to achieve optimal system performance, the nature of plasma-surface interactions under conditions of interest to space power and thrust devices must be understood both qualitatively and quantitatively.

In order to carry out this study, metal and dielectric samples can be mounted in the downstream flow from a quasi-steady MPD arcjet whose plasma properties (temperature, composition, flow speed, density) are known and can be varied by varying the location of samples in the plasma stream and by varying the power to the arcjet and the propellant gas from which the plasma is formed. As shown in Fig. 1, the samples can be mounted with their surface planes parallel or perpendicular (facing upstream or downstream) with respect to the plasma flow. This geometry and mounting location, convenient to optical and access ports in the vacuum vessel, constitute an ideal arrangement for detailed diagnostic work.

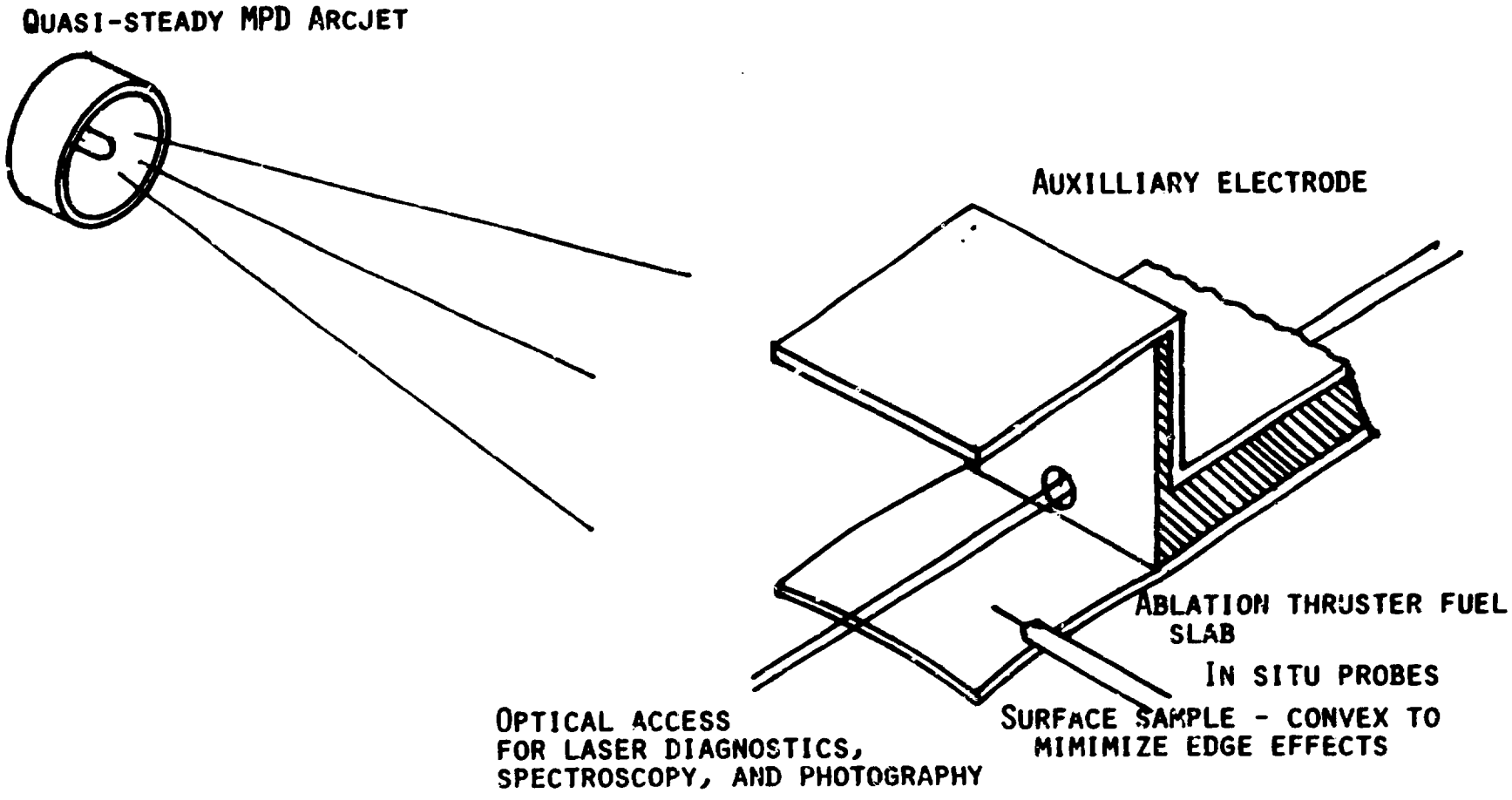

FIG 1. SCHEMATIC OF PLASMA SURFACE INTERACTION EXPERIMENTS

III. SCIENTIFIC DEFICIENCY

In a useful review paper (Ref. 1) F.G. Baksht and V.G. Yur'ev discuss theoretically some of the lengths of interest in plasma-solid interaction: the Debye length that defines the zone of non-neutrality separating a material wall from the plasma; the Langmuir sheath length that describes the expanded region of space-charge present when a current flows to the electrode; the energy relaxation length for formation of a Maxwellian distribution for the electrons; the recombination length over which an equilibrium between ionization and recombination is established; and the temperature relaxation length over which the heavy particle component of the plasma relaxes to the electron temperature to complete the thermal equilibrium. These lengths and their ordering, which depend on the mean free paths for interaction between electrons, ions and neutrals, define the physical processes that take place in the sheath. This manner of conceptualization provides a very convenient scheme for understanding electrode and wall phenomena. Experiments to show the effect of electrode geometry, material, surface preparation, etc., on the details of sheaths and boundary layers have not been carried out. The experimental understanding of these phenomena is necessary since processes in practical power and thrust devices are blended in a highly non-linear way that precludes accurate prediction on the basis of simple theory. The theoretical tools that one needs to understand experimental data are at hand; what is lacking are the data, gathered in such a way that simultaneous processes can be disentangled and device-specific phenomena recognized as such.

IV. PROGRESS

In order to be able to operate the MPD arcjet for ten's of microseconds without a significant degradation of the overall vacuum, it was necessary to construct a large vacuum tank. This tank is a stainless steel cylinder, 6 meters long with a 61 cm inside diameter. The total volume is 1460 liters. The tank has two coaxial 35.6 cm diameter diagnostic ports for an optical clear view through the test section, and one 15.2 cm diameter port orthogonal to the other two. In addition, there is an electrical feed-through port and two 7-inch diffusion pump ports at opposite ends of the tank. The vacuum pumping equipment consists of one mechanical roughing pump, a Welsh Duo Seal Model 1375, rated at 1000 liters/min, two 6-inch oil diffusion pumps and two backing pumps. Each diffusion pump is topped with a 7-inch gate valve and a liquid nitrogen cold trap with a pumping speed of 2000 liters/sec for water vapor. The oil diffusion pumps are also rated at 2000 liters/sec. The base vacuum of the system monitored by ionization gauges, is of the order of 10^{-6} Torr. The general layout of the tank is shown in Fig. 2.

The energy storage system and pulse forming line to power the MPD arcjet consists of a 5-section voltage-fed synthetic transmission line having a 0.75 Ohm characteristic impedance. The total energy storage is 22.5 kJ with the capacitors charged to 20 kV. The output pulse risetime and decaytime is 8% of the design pulse width of 185 μs. At maximum operating voltage, the short-circuit output current is 27 kA. The pulse-forming network inductors consist of a single-tapped solenoid wound on a 14.6 diameter nylon rod. The system is switched by a single GI-37407A ignitron triggered through a 1:1 aircase isolation pulse transformer. The primary winding of this transformer is driven by a 6-stage SCR Marx generator which is in turn triggered via TTL logic with selectable internal delay timer and corresponding sync outputs to provide appropriate time delays for diagnostics. The capacitors are mounted on individual shelves in a portable shielded steel enclosure and are connected to the pulse-forming

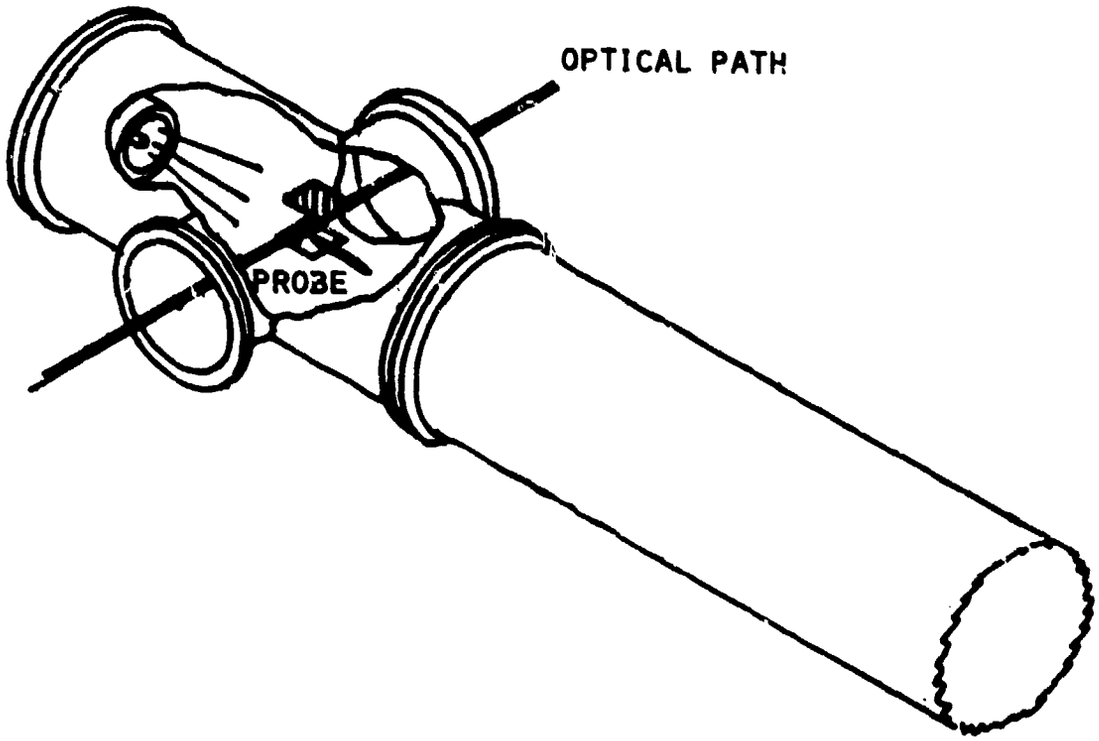

FIG 2. VACUUM TANK WITH ARCJET AND SAMPLES

network inductor through 6 mm copper tubing. A current shunt at the output of the pulse-forming network allows the output current to be measured.

Using a modified Princeton design, an MPD arcjet was fabricated to serve as the prime plasma source for the plasma-surface interaction experiments. This device has a 2 percent thoriated tungsten cathode (center electrode) of 15 mm diameter and an anode of oxygen-free copper. Gas is admitted through a series of ports in a ceramic insulator. This arcjet, shown in Fig. 3, is ready for installation in the vacuum system in time for the second year of effort.

While the MPD arcjet was being fabricated, a railgun triggered by a pulsed plasma thruster was installed and preliminary diagnostic measurements were made. (This work coordinated well with a separate project for AFRPL on a new thruster concept). Magnetic probes were constructed using 40 turns of #38 insulated copper wire wound on a 1 mm diameter mandrel. The coil leads were tightly twisted. The coil was then removed from the mandrel, and impregnated with polystyrene, and then cemented onto an acrylic rod to insure constant orientation. The coil-tipped rod was then inserted into a 3 mm OD pyrex sleeve, sealed at one end. The axis of the field-sensing coil is perpendicular to the axis of the pyrex sleeve. The probe signals were integrated by a 100 MHz band width balanced differential integrator having an equivalent 6-7 μs integration time constant. For calibration, the railgun was shorted at the muzzle end and the time resolved response of each probe was recorded along with the output of the capacitor bank/pulse-forming line. In this way a matrix of in situ calibration factors was obtained for various probe locations. The short was now removed and a set of time-resolved probe responses was obtained between 10 and 16 cm downstream from the railgun breech for probe channel penetrations of 1, 2, and 3 cm. These are shown in Fig. 4 as percentages of the calibration signal at times corresponding to beginning, midpoint, and tail end of the pulse.

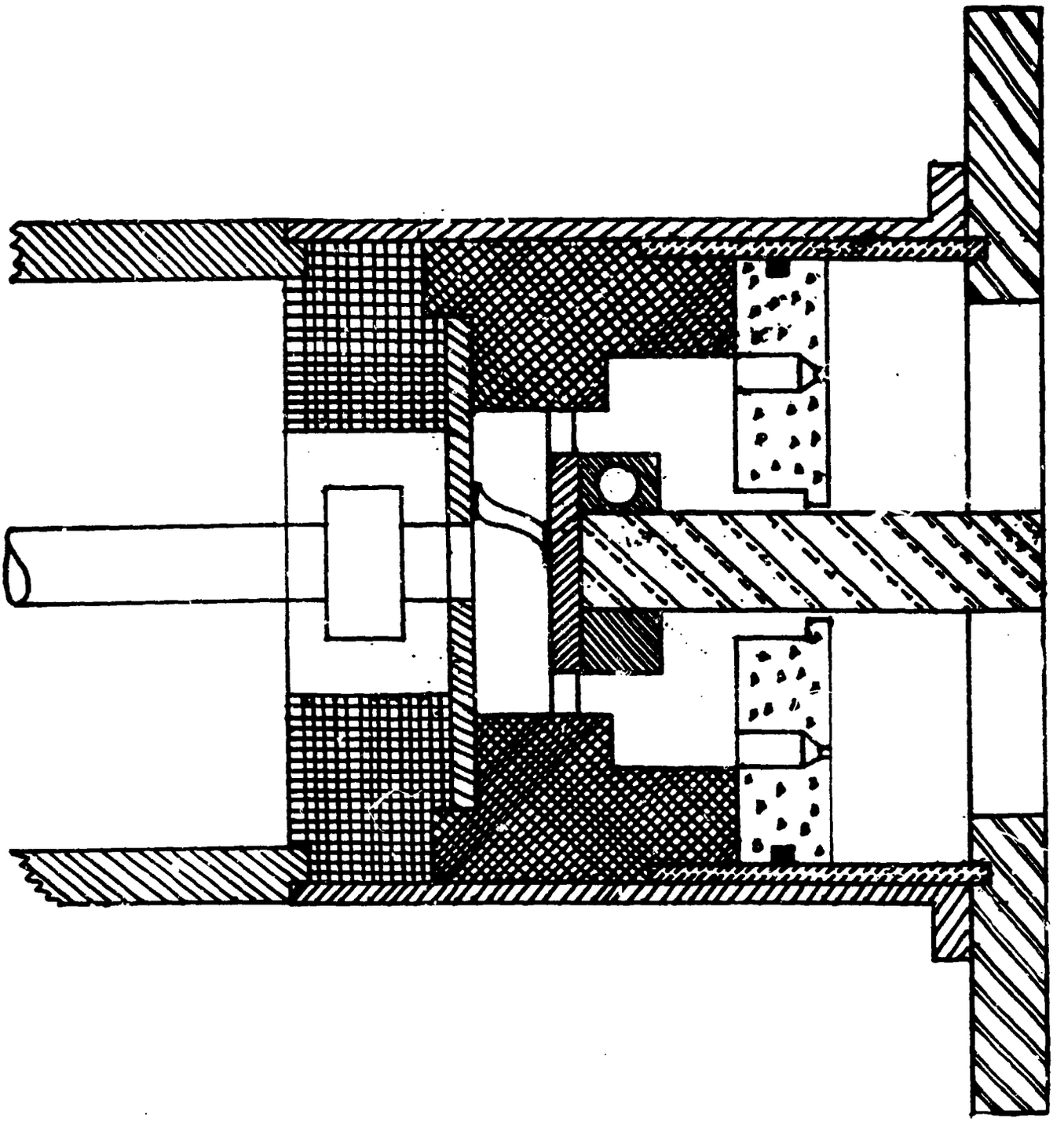

FIG 3. MPD ARCJET

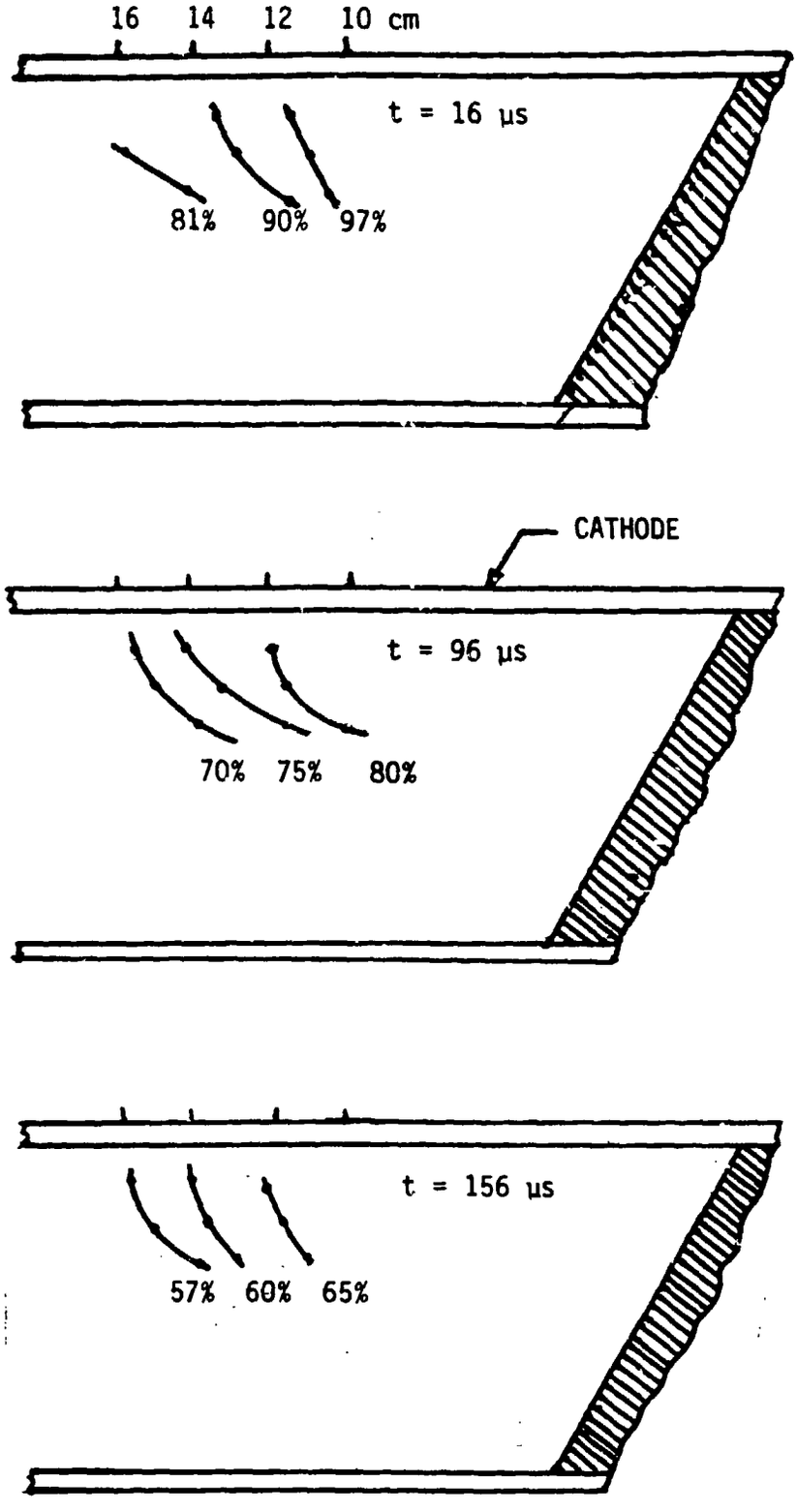

FIG. 4. CURRENT DENSITY CONTOURS.

Initial spectroscopic efforts have also been made on the railgun-pulsed plasma microthruster source. Using a 1.2 meter spectrometer, the relative intensity of the Hα line and the 4810.14 Å line of zinc were measured as a function of distance from the cathode. The results of these measurements are shown in Fig. 5. Figures 6 and 7 show the time-resolved relative intensity of the hydrogen and zinc lines respectively. Preliminary interferometric measurements on the railgun/PPT plasma have been made using a He-Ne cw laser. These measurements indicate an average number density of 3×10^{14} cm^{-3} near the muzzle of the railgun.

Measurements have been made downstream of the railgun using single-electrode Langmuir probes. The shot-to-shot reproducibility was sufficiently good that, by placing the probes at different longitudinal stations, being careful not to put the downstream probe in the wake of the upstream one, plasma directed velocity could be measured. This was about 3 cm/μs. Owing again to the good reproducibility, it was possible to measure the slope of the current-voltage curve and determine the electron temperature to be about 7 eV. Measurement of the saturation current for both ions and electrons yielded a plasma density of 10^{13} cm^{-3} which is consistent with the order of magnitude higher density measured upstream.

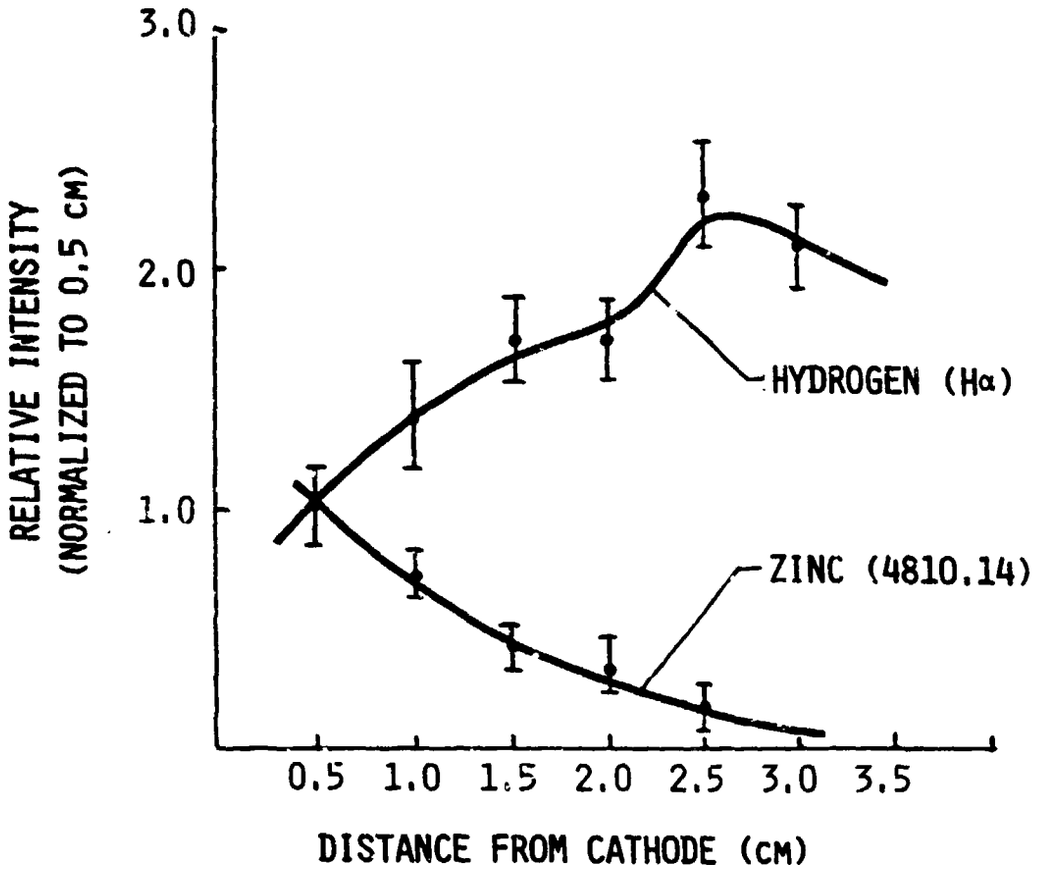

FIG 5. RELATIVE INTENSITY OF H AND ZN NEAR CATHODE

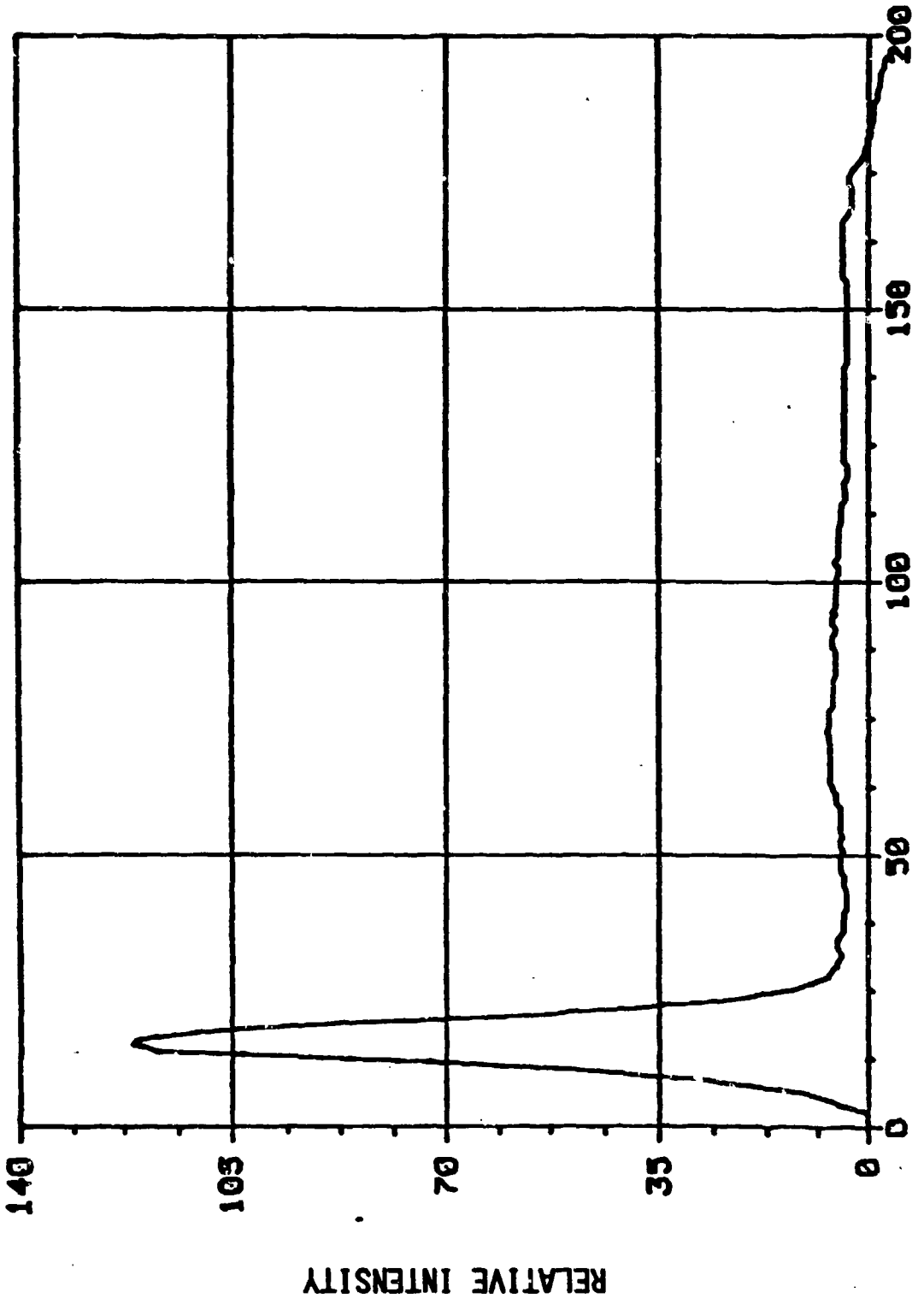

FIG 6. TIME-RESOLVED Hα (656.3 NM) INTENSITY

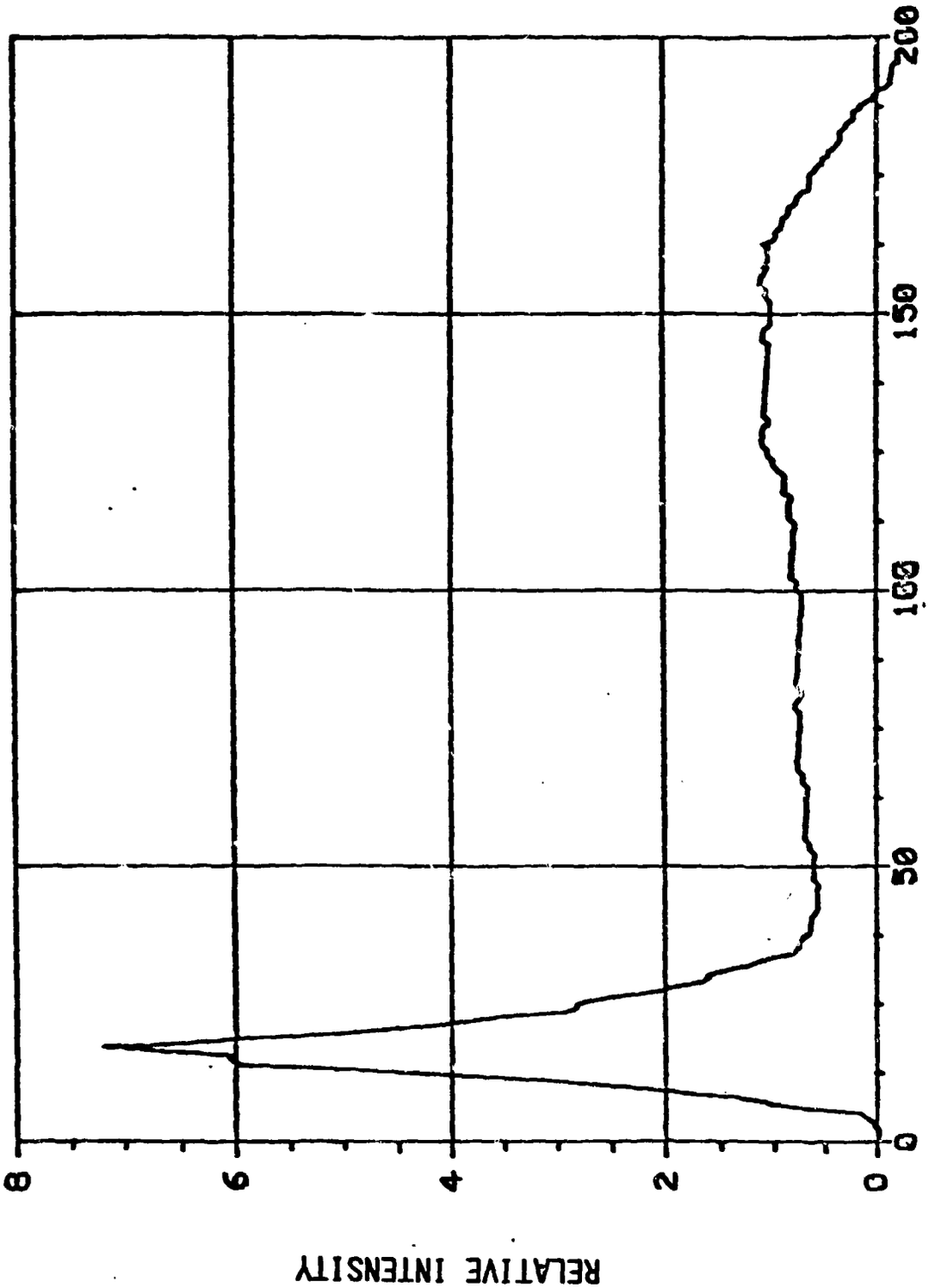

FIG 7. TIME-RESOLVED ZnI (481.05 nm) INTENSITY

V. DISCUSSION

The study of plasma-surface interactions in specific devices faces a several difficulties. Separate physical phenomena may occur coincident in space and time as a result of features peculiar to the device or the electrical pulse used with it. Also, the geometrical arrangement of MHD channels and coaxial thrusters precludes convenient diagnostic access. For these reasons, we are examining plasma-surface interactions under conditions that allow individual physical processes to be delineated and in a geometrical arrangement where diagnostic access is optimized. For example, having explored the downstream properties of the MPD arcjet plasma in the absence of samples, we can then introduce various samples with their planes parallel to the plasma flow and measure, by spacially-resolved diagnostic methods, the variation of ion and electron temperatures, density, and composition as the surface of the sample is approached. By using telescopic optics and making the surface of the sample slightly convex to avoid looking through edge effects, the effects of heat transfer to the sample in a viscous turbulent boundary layer can be measured as well as the scale of the vorticity associated with the boundary layer. Current flow to the metallic sample can then be applied to see the effects of charge transfer. The current can also be made to flow along the face of the insulator samples in order to study ablation. The current level can be increased from a value where no local plasma acceleration is experienced to a value where the Lorentz force produces a strong perturbation on local conditions. By varying power to the MPD arcjet, type of gas supplied to the jet, sample material and geometrical arrangement, and electrical power supplied to the samples, the whole range of plasma-electrode-insulator interaction phenomena of interest can be modeled.

The Debye length that scales the thickness of the non-neutral layer separating a wall from the body of the plasma will be much less than the characteristic dimension of surface roughness of the wall for most cases of interest. For local high temperatures and/or lower densities, these two lengths could

become comparable which would lead to highly non-uniform electric fields and the likelihood of fine cathode spots and enhanced erosion. Large cathode spots can also appear at higher densities owing to instability in the formation of the current sheet. This concentration of the current to some critical current density then leads to local heating of the cathode to the point that electron emission is strongly enhanced and the arc settles into a stable cathode spot. In this way, enhanced erosion due to spot formation may be the result of hydromagnetic instability or entry into a critical regime of density and temperature for a given total current.

The nature of the cathode emission mechanism is also of great interest. For work functions of cathode materials much less than the ionization potential of plasma ions incident upon the cathode, the chances are good that the impacting ion will capture an electron from the cathode and be re-emitted diffusely as a neutral which may then be reionized in the body of the plasma just outside the cathode fall zone. After breakdown, the voltage across the current sheet may be 100 volts or so, whereas the energy necessary to ionize the re-emitted atom may be of the order of 50 volts when all associated processes have been taken into account. Moreover, if the densities are sufficiently low such that the incoming ion can carry its high speed associated with the directed energy of the plasma into the cathode, then, owing to the diffuse re-emission, this component of momentum will be lost and the result will be a severe viscous drag on the plasma. This will not occur, however, if the flow is collisional outside the boundary layer; in that case the axial momentum of the ion will be lost before it reaches the cathode surface. If the plasma density is high ($n > 10^{17}$ cm^{-3}) and is composed mostly of high-Z material, then a sufficient flux of photons with energies above the photoelectric threshold may be available to cause electron emission by photoelectric effect. Thus there may exist an optimum point in operating efficiency that depends on the balance of emission mechanisms.

It may not be practical to adjust the balance of emission mechanisms by optimizing the atomic number of the plasma. Instead, it may be possible to rearrange the ordering of various characteristic lengths. For example, if atoms of cathode material could be ionized before exiting the boundary layer, then they could return to the surface quite near their point of origin such that the roughening and erosion of the surface might be reduced (for a homogeneous cathode material).

The Debye and Langmuir sheath thicknesses as well as the viscous boundary layer thickness all scale as $1/n_e^{\frac{1}{2}}$. The mean free path for ionization scales as $1/n_e$, thus higher electron densities near the cathode are more likely to lead to conditions favorable to retaining neutrals emitted from the surface. The question is, can we achieve enhancement of electron density near the cathode? The answer to that question may explain why the MPD arcjet appears to enjoy such a favorable mode of operation. In this device, the cathode which is the outer coaxial electrode experiences a plasma flow onto the cathode surface owing to the geometrical arrangement of the device. Thus the electron density in the cathode sheath will be enhanced over free-stream values. We can test this idea with our surface samples in an optimal geometry for diagnostics.

This can be done by orienting the entrance slit of our spectrometer perpendicular to the surface of the sample and intersecting it. We will then observe the spectral lines of various species to have different heights depending upon the mean free path for ionization. With good telescopic optics the spatial resolution can be quite fine. We can examine the mean free paths of different species in a single event by employing alloy samples. Brass would not be a particularly good choice since copper and zinc are so similar in mass, however 5 kt. gold would do quite nicely. By measuring the relative intensity of Au and Cu spectral lines as a function of distance from the cathode and as a function of time using the framing and streak cameras, we should be able to gain information on the electron

density profile near the cathode surface and may be able to visualize the local flow field in some detail.

Figure 8 depicts a sample located at arbitrary orientation to the flow from an arcjet. The sample is mounted on an x-y translation stage with remote vacuum feedthroughs so that sample position can be changed without breaking vacuum. Spectral emission from ablated surface atoms and from the ambient plasma is observed normal to the sample surface with a high resolution spatial-temporal spectroscopic system. The spectroscopic system consists of a simple lens, two turning mirrors mounted on an x-z translator, a 1.2 meter visible spectrograph and output to either film, photomultiplier tube, or the RDA microchannel plate amplified fast framing camera. Spatial resolution of less than 100 microns is provided by movement of the turning mirrors and/or by the use of the movable slit mask as shown.

In the early phase of the next year's work (second year of the three-year program), the MPD arcjet powered by the 20 kJ pulse-forming network will be installed in the tank and the flow velocity, density, and temperature of the downstream plasma will be determined as a function of space, time, and energy supplied to the arcjet. In addition, the radiation from the plasma will also be determined as part of the general environment in which the samples will be tested. A separate power source (capacitor bank) will provide current and voltage to the metallic surface samples for tests involving electromagnetic interactions ($\vec{J} \neq 0$). Electrodes mounted on either side of a dielectric surface can be used to provide current parallel to the plane of the surface, with changes in the orientation of $\vec{J} \times \vec{B}$ (relative to $\hat{n}$) achieved by varying the return path of the current-carrying circuits. Similarly, electrode interactions can be studied by using an auxilliary electrode appropriately configured to avoid disturbing the experimental conditions near the metallic test sample. Changes in relative magnetic pressure would follow from changes in the current level at the surface, holding the plasma pressure constant. Magnetic Reynolds number R_m would be varied by changing the dimensions of the sample and/or the flow speed.

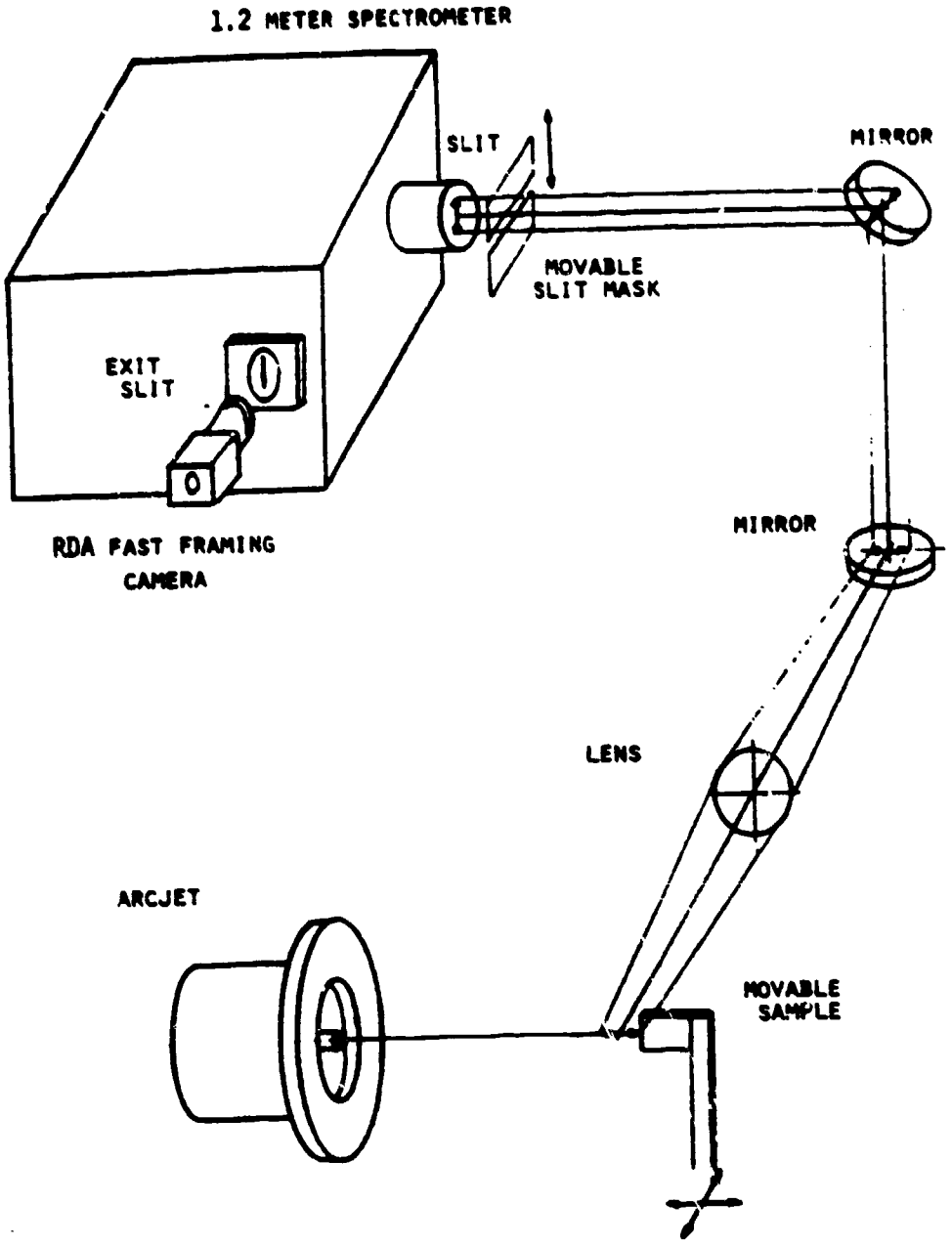

Fig. 8. This shows a schematic of the optical diagnostic access to the surface sample. The slit mask defines the spatial resolution, the spectrometer provides wave length resolution, and the RDA camera provides time resolution.

The diagnostic techniques used in the study include:

1. Optical photography - RDA has assembled a two-frame micro-channel plate image intensifier camera system that will have a resolution of 25 line pairs/mm and a variable exposure time of 5 ns to 100 ns with any desired inter-frame delay. The light gain is $7\text{-}15 \times 10^3$. In addition, we have purchased a Hamamatsu streak camera with 20 ns to 500 μs streak time per full frame and a light gain of 3×10^3. These instruments, purchased with RDA money, will be used to observe the plasma flow relative to the samples and to observe the formation of luminous boundary layers near the surface under various test conditions.

2. Optical spectroscopy - will be used to identify the composition of the plasma near the surface. For sufficiently strong lines spatially-resolved spectroscopy will be employed and the Hamamatsu streak camera will be used to gain temporal resolution. Line broadening techniques will be used to corroborate density and temperature measurements obtained by other means.

3. Laser diagnostics - A cw laser will be used as the light source for schlieren, interferometry and light absorption measurements.

4. Langmuir probes - will be used to monitor the plasma potential near the test surface. Measurements of potential difference between local plasma and electrodes provides the fall voltages associated with current conduction. Differences in potential within the plasma can be used, under certain conditions, to provide information about electron pressure gradients and local flow speeds.

5. Magnetic probes - will be used to map the magnetic field distribution and thereby to infer current densities as a function of space and time in the plasma. Segmentation of an electrode surface might be used to estimate the space and time behavior of current conduction to the surface.

6. Piezoelectric pressure probes - will enable the measurement of static and dynamic pressure in transient plasmas. These

measurements will probably be useful only as a secondary corroboration of data obtained by other means, however, in light of the modest effort, it is worthwhile.

7. Bolometer - bolometric measurements of UV flux to the metallic sample surfaces will be used to correlate other data on the electron emission mechanism from cathodes.

For each combination of sample and plasma material, plasma parameters, and interaction mode, the above range of diagnostic techniques will be applied in an attempt to measure each quantity by two independent means. In this way data will be collected that will enable conclusions to be drawn concerning refinements in the design of space power and thrust devices. It is anticipated that the basic energy exchange processes associated with charge and mass transport at plasma-solid interfaces will be delineated in the course of these measurements. The cathode fall will be measured as a function of local plasma density. The balance between ion impact and photoelectric effect under conditions applicable to pulsed and quasi-steady electric thrusters will be clarified. On the basis of these findings, means and methods will be developed in the third year of this contract whereby efficiency and lifetime of space power and thrust devices may be optimized.

The effort in the present year will be focused on measuring downstream properties of plasma from the MPD arcjet and taking data on the surface samples. The third and final year will be devoted to completing the data collection and, in conjunction with theoretical modeling, to applying the results to device-specific problems.

We might note that with the MPD arcjet in place and a battery of formidable diagnostics at hand, it would make good sense to explore the plasma properties inside the arcjet even though this effort would represent a digression from the main object of the plasma-surface interaction study. Formation of

the current sheet, homogeneity of the current distribution, temperature, composition and density distribution, could all be studied since the geometry of the MPD arcjet, while not as ideal as that envisioned for the surface samples, is not overly restrictive for diagnostics.

VI. REFERENCES

1. F.G. Baksht and V.G. Yur'ev, Sov. Phys. Tech. Phys., 24, 535 (1979). This is a lengthy review paper of mostly Russian work on electrode phenomena in low-temperature plasmas and is appropriate to MHD generators, arc devices, plasma accelerators, and thermionic diodes. This is a valuable reference which reviews quantitatively the state of knowledge of electrode-plasma interaction effects associated with potential and density distributions, current flow, electron thermalization, near-electrode ionization, etc.

2. I.I. Beilis, Teplofiz. Vys. Temp., 16, 848 (1978). This work shows that cathode erosion by slowly moving arc spots in a MHD generator was determined by the emission properties of the cathode. This paper goes on to establish effective work functions for metal cathodes covered with potassium seeding material.

3. A.M. Vasyutkin, Teplofiz. Vys. Temp., 17, 874 (1979). In this work, applicable to MHD generators, the author shows that the temperature distribution in the electrode sheath and the thickness of the sheath is such as to favor the transfer of heat onto the electodes. He establishes that the voltage drop is proportional to the power dissipated in the sheath and examines the mechanism as associated with the generated current passing through the inhomogeneous boundary layer.

4. N.N. Baranov, A.E. Buznikov, and V.I. Kovbasyuk, Teplofiz. Vys. Temp., 19, 857 (1981). Spatial nonuniformities of electrical parameters in a MHD generator are correlated with nonlinear phenomena in the electrode sheath.

5. M.F. Zhukov, et al, Sov. Phys. Dokl., 26, 907 (1981). This paper reports a spectroscopic study carried out in a coaxial arc in which the dynamics of evaporated electrode material in the sheath and the interaction of this vapor with the adjacent plasma were examined.

6. N.A. Sanders and E. Pfender, J. Appl. Phys., 55, 714 (1984). This paper reports a detailed study using Langmuir probes of the anode fall in constricted and diffuse argon arcs. The currents involved are of the order of 10^2 amps with electron temperature somewhat less than 1 eV.

7. R.C. Oberth and R.G. Jahn, AIAA Journal, 10, 86 (1972). In this study of a quasi-steady MPD arcjet, the authors find that the fractional power loss to the anode is an inverse function of the arc power. The effect of underfeeding the propellant gas to the discharge is shown to be enhanced erosion and the development of intense electric fields around the anode in order to compensate the lower plasma density.

8. A.J. Saber and R.G. Jahn, AIAA Journal, 16, 328 (1978). The correlation of fractional anode power loss to arc power is examined quantitatively and it is shown that the power loss decreases from 50% at 200 kW to 10% at 20 MW. A theoretical model shows that this is due to the smaller mean free paths in the plasma at high powers which partially decouples the heat conduction into the anode sheath.

9. K. Thom, J. Norwood, and N. Jalufka, Phys. Fluids Suppl. 7, 567 (1964). The authors argue that ion impact on the cathode of a coaxial plasma gun and the subsequent diffuse reflection of a neutral into the plasma cause an effective viscous drag that limits the attainable plasma velocity under conditions of low density.

10. C.T. Chang, Plasma Phys., 13, 1067 (1971). This paper discusses the effect of wall friction on the current-sheet speed in a magnetically driven shock tube and concludes that the experimental results are consistent with the mechanism proposed in Ref. 9.

APPENDIX

"Multi-Stage Plasma Propulsion"

by

P.J. Turchi, C.N. Boyer, and J.F. Davis

in

Proceedings of the 17th IEPC
Tokyo, 1984

This paper resulted from the use of diagnostics and facilities developed under both AFOSR and AFOSR sponsorship.

IEPC '84

IEPC 84-51
Multi-Stage Plasma Propulsion

P. J. Turchi, C. N. Boyer and J. F. Davis,
Washington Research Lab., Alexandria, VA, USA

JSASS / AIAA / DGLR

17th International Electric
Propulsion Conference, Tokyo, 1984

MULTI-STAGE PLASMA PROPULSION

P.J. Turchi, C.N. Boyer and J.F. Davis
R & D Associates
Washington Research Laboratory
Alexandria, VA USA

Abstract

A strategy for introducing electric propulsion into the U.S. inventory of techniques for near earth missions utilizes the space-operational pulsed plasma microthruster (PPT) in conjunction with additional stages of acceleration and/or mass addition. Such multistage plasma propulsion would allow thrust power to increase with the increased availability of space-electrical power, without having to change thruster physics. Theoretical considerations suggest possible modes of operation, including the transition from slug acceleration to surface ablation by varying the electrode dimensions. A series of experiments are also reported that explore three thrusters, comprising pulsed acceleration of PPT plasma to 4 x 10^4 m/s by a long second stage-thruster, and quasi-steady ablation of additional Teflon plasma in second-stages with short electrodes. The latter thrusters provide plasma speeds of 1.7-2.5 x 10^4 m/s with nearly constant average particle fluxes for the duration of the current pulse (150 μsec after the PPT transient).

Introduction

The development of a family of electric thrusters based on the pulsed plasma microthruster (PPT) involves the use of additional stages of electrical energy input[1]. There are two basic approaches. The initial plasma from the PPT can be accelerated to a higher average speed to achieve higher specific impulse and greater system efficiency. Alternatively, the PPT exhaust stream can be used to initiate an electrical discharge over an insulating surface to increase the system mass flow by ablation, thereby increasing the total system thrust. In both approaches, to avoid additional switching, the stages subsequent to the PPT would be activated by the arrival of the PPT plasma. Variations in current pulse duration and geometry would allow the envisioned family of thrusters to comprise simple plasma slug accelerators, pulsed thermal arcjets, and quasi-steady MPD arcjets. In the last instance, the use of ablation to create the necessary mass flow would allow operation without repetitively pulsed propellant valves. The present paper reports recent theoretical and experimental efforts at the RDA Washington Research Laboratory examining various aspects of multistage plasma propulsion. Theoretical discussions range from simple slug acceleration modeling to consideration of distributed plasmas and currents. Experimental work tests three examples of second-stage thruster operation.

Acceleration of the PPT Plasma

The simplest form of multistage plasma propulsion consists of the PPT injecting a slug of plasma between two rail-electrodes that are connected to a charged capacitive power source. The capacitive source could be trickle-charged between PPT firings (in the manner of a photographic flash attachment) and could utilize capacitor elements of the same type used previously by microthrusters on actual long term space missions. If the PPT exhaust is directed in a perpendicular fashion across the rail gap (Fig. 1a), then the PPT merely provides mass (and a means of initiating current flow in the second-stage). The kinetic energy of the PPT exhaust is thus discounted in this example. Acceleration of the injected plasma along the rails is described by the usual set of lumped-circuit equations in which the electrical impedance of the accelerating plasma discharge is expressed as the rate of change of circuit inductance. By nondimensionalizing the equations, a single dimensionless parameter is obtained that determines the discharge dynamics:

$$\beta = \frac{E_o F^2}{MZ^2}$$

where E_o = initial capacitor energy
F = inductance change per unit length of plasma motion
M = plasma slug mass
$Z = (L_o/C)^{\frac{1}{2}}$ = initial circuit impedance

In Fig. 2a, the kinetic efficiency, $\epsilon = \frac{1}{2}mu^2/\frac{1}{2}CV_o^2$, (for an exhaust speed $u = \beta\omega Z/F$ developed in the second-stage thruster) is seen to rise quickly as the dimensionless dynamic parameter β is increased to about $\beta = 3$; less rapid gains are achieved with higher values of β. (In these calculations, the dimensionless speed, ω, achieves its peak value before the computation is ended).

If the PPT plasma is directed parallel to the rails, ($\omega = \omega_o \neq 0$) but spread across the rail gap to initiate current flow, as shown in Fig. 1b, then higher efficiencies are obtained because the moving plasma presents a higher initial (dynamic) impedance to the power supply. As shown in Fig. 2b, the kinetic efficiency

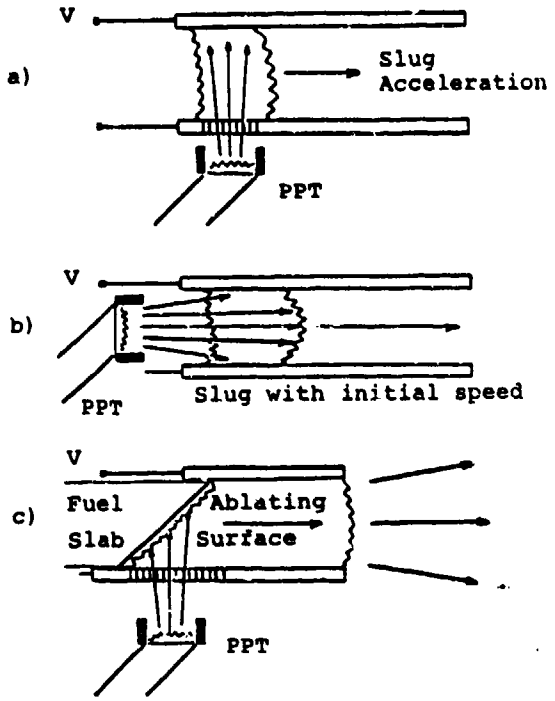

Fig 1 - Conceptual diagrams of plasma injection from PPT into second-stage thruster:
a) injection acrcss gap (eliminating PPT momentum;
b) injection along electrodes to increase initial dynamic impedance;
c) injection along second-stage insulator to initiate ablation for mass-addition.

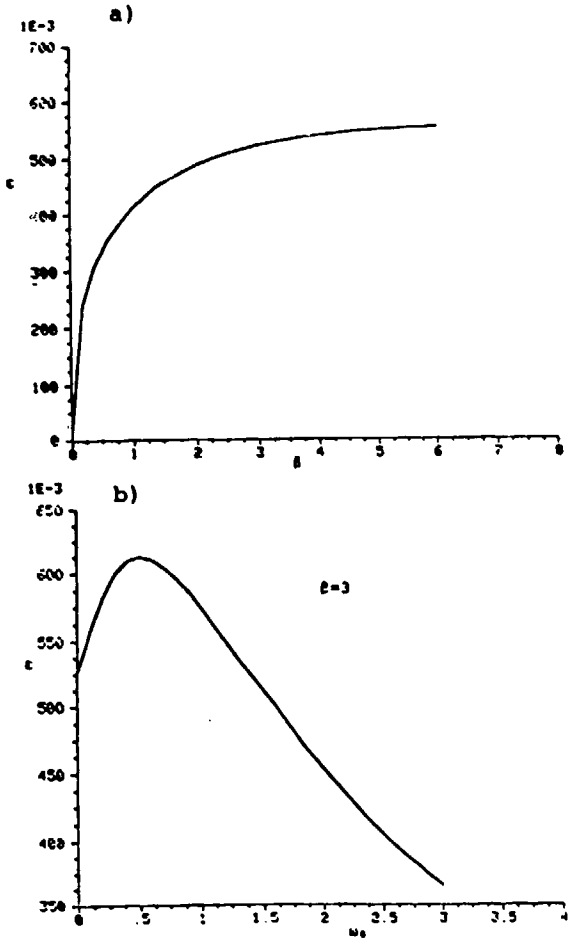

Fig 2 - Results from normalized lumped-circuit calculations:
a) Efficiency of plasma slug acceleration versus dimensionless dynamic parameter β for case of zero initial streamwise motion.
b) Efficiency of plasma slug acceleration versus initial normalized speed $\omega_o = u_o F/Z\beta$, for case of β =3. Flow speed doubles in the second-stage for ω_o = 0.3t.

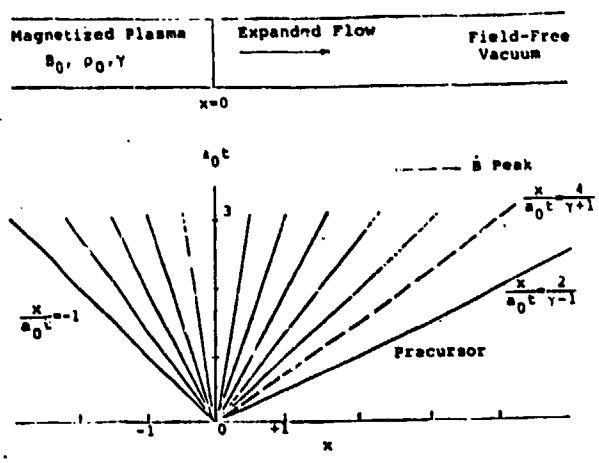

Fig 3 - Expansion of a semi-infinite magnetized plasma into a field-free vacuum. A centered expansion fan in the xt-diagram shows the spread of the current conduction region with time.

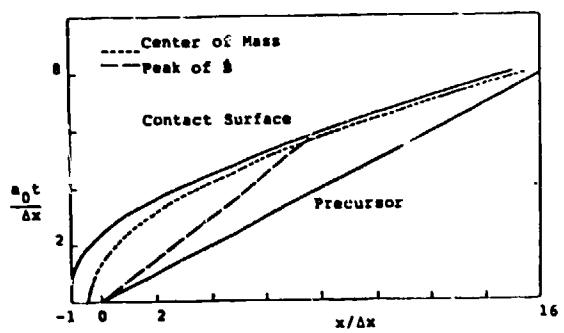

Fig 4 - Expansion and recollection of a plasma slab driven by a constant magnetic field. The contact surface indicates the boundary between high density plasma and vacuum if the PPT injection could stop abruptly.

$\epsilon = \frac{1}{2}\beta(\omega^2 - \omega_o^2)$ can exceed 55% , while doubling the exhaust speed of the plasma slug(ω_o = .36); the results shown are for β = 3. In dimensional variables, the simple slug acceleration model indicates that specific impulse values in the range of 1500 sec should be possible with system efficiencies in excess of 50%. Such values are not especially remarkable for electric propulsion techniques, but are encouraging as improvements on an existing space-tested thruster.

For near term missions (i.e., near earth vs outer planets), the optimum specific impulse based on available specific power values ($\alpha \approx 30$ w/kg) will probably not exceed 2000 sec. The primary virtue of electric acceleration of the PPT exhaust plasma, therefore, is improved thrust efficiency. Such improvement has two aspects: 1) the increase in time-averaged dynamic impedance associated with acceleration of an initially moving plasma; and 2) the preferential acceleration of slower plasma that is emitted later in time by the PPT. The latter aspect recognizes that the PPT tends to provide two components of plasma. A fast component due to the PPT discharge is observed to exit the microthruster followed by a slower component associated with the continued ablation of the PPT fuel surface. The specific impulse is thus obtained as a temporal average over flow speeds that are higher and lower than optimum; it would be useful to reduce the velocity spread to achieve higher system efficiencies.

Acceleration of the distributed PPT plasma in the second-stage may be considered in terms of expansion of magnetized plasma. In Fig. 3, a semi-infinite plasma ($x \leq 0$) is allowed to expand into a field-free vacuum ($x \geq 0$). The plasma density may be calculated at any time and position from adiabatic expansion through a centered expansion fan. If the plasma resistivity is low, the magnetic flux will tend to convect with the plasma mass, so the spreading density gradient will correspond to a current distribution. At x=0, sonic conditions are maintained, so the downstream evolution of the plasma discharge can be modeled by the downstream expansion fan even if the semi-infinite magnetized plasma is replaced by a source of plasma from the PPT. (Resistive diffusion at the entrance to the second-stage is necessary to extract magnetic flux from the second-stage power circuit). The expansion fan analysis then indicates that about half the current will be carried in the downstream plasma discharge, while the remainder will flow near the inlet to the second-stage. If the injected flow density drops substantially, then a "contact surface" between the previously injected plasma and this low density flow will accelerate and sweep up the earlier plasma. For sufficient length of rails (about 15 times the effective "length" of the injected PPT plasma) a single plasma slug would exit the second-stage. The expansion and recollection of plasma in the second-stage is depicted in Fig. 4.

If the rail length is significantly less than the distance needed to recollect the plasma, then it would be more appropriate to consider magnetic diffusion (vs adiabatic expansion) as the mechanism establishing the discharge distribution. With proper insulation, acceleration of the plasma will cease slightly beyond the end of the rails and all the plasma injected into the second-stage should experience about the same change in momentum. To the extent that this momentum change is much greater than the initial momentum of the slower component of the PPT exhaust, the second-stage should exhibit a more uniform exhaust velocity and thereby achieve higher efficiency at a desired specific impulse level.

Generation of Higher Thrust at Fixed I_{sp}

To obtain higher thrust at a fixed value of specific impulse, mass addition is necessary. A conceptually simple approach utilizes the PPT to initiate an arc over an insulating surface that then ablates due to the heat flux from the plasma discharge (Fig. 1c). The mass flow into the discharge thus depends on the local plasma current density, which in turn depends on the flow through the discharge. The physical situation resembles the flame zone over a solid propellant surface and will depend quantitatively on the details of the electrical resistivity and thermal conductivity of the flow as it changes from vapor to highly ionized plasma. Some qualitative insight, however, for purposes of the present discussion, may be obtained by examining the equations governing the discharge distribution downstream of the region of plasma formation.

The basic equation for the current distribution may be written as a balance of convection and diffusion of magnetic field:

$$\frac{D_e}{Dt}\left(\frac{B}{\rho}\right) = \frac{\eta \nabla^2 B}{\rho \mu}$$

where the convective derivative is based on the electron fluid speed and a constant resistivity η downstream of the "flame zone" has been used for simplicity. If the plasma density is sufficiently high (electron current drift speed << plasma flow speed), then the plasma flow speed can be substituted for the electron fluid speed (thereby eliminating tensor current flow and electrode polarity effects from the MHD analysis); the electron pressure gradient term has already been neglected in the generalized Ohm's law used to obtain this equation.

In steady-state, and allowing only one dimension of spatial variation (i.e.,

streamwise), the convective vs diffusive balance becomes:

$$\frac{d}{dz}(uB) = \frac{\eta}{\mu}\frac{d^2B}{dz^2}$$

where a uniform mass flow, $F=\rho u$, is invoked in order to eliminate mass density from the equation. In solving this equation, the streamwise location of the downstream boundary value (B=0) is specified (or computed). If this location is specified, for a given upstream boundary condition ($B=B_1$ at $z=\delta$, the downstream edge of the flame zone), then the current density corresponding to the current in the downstream region is determined. Higher flow velocity tends to convect magnetic flux downstream, increasing the current density near the B=0 location at the expense of upstream positions ($z>\delta$). The current density, resistivity, and uxB at $z=\delta$ then provide the electric field that sets the volumetric heating rate of the plasma near the ablating surface. A portion of this heating supplies the energy needed for ablation and ionization, thereby scaling the mass flow rate. The lower the mass flow rate, the higher the flow speed for a given magnetic driving pressure and the greater the tendency to concentrate portions of the current near the downstream B=0 boundary location and in the flame zone. (Ablation driven by increased resistive heating in the "flame zone" can then compensate by raising the mass flow rate).

For a given maximum magnetic field (i.e., total current), placement of the B=0 boundary further downstream lowers the current density and thereby lowers the dissipation that is providing mass flow to the plasma discharge. Thus, if the electrode rails of the second-stage are too long, ablation of the second-stage propellant slab may be insufficient during the current pulsetime from the power supply. Starvation of the discharge may then lead to electrode erosion (which is not the desired mechanism for mass addition). Such starvation may be mitigated by the continued influx of slower material from the PPT. The operation of the second-stage, however, would then resemble the expansion-acceleration mode discussed in the previous section.

Proper operation of the second-stage to provide mass addition therefore requires the minimum length of electrode rails consistent with the lateral dimension of the PPT exhaust. Since it is often the case that currents can be sustained in plasma flows that serve as extensions of physical (solid) electrodes, it is also important to avoid accelerating the PPT exhaust plasma out of the second-stage before ablation can replace the PPT mass flow. The rise time of current in the second-stage, therefore, should approximately match the pulsewidth of the PPT exhaust. Too short a risetime can lift off a current sheet of PPT plasma (plus initial ablation) from the insulator (in the manner sought for successful operation of some pulsed plasma guns). If the risetime is too long, however, the PPT plasma may splash downstream and severely shunt the insulator surface discharge.

Experimental Tests

Three experimental test series on multistage plasma propulsion have been conducted at the RDA Washington Research Laboratory. The first series corresponds to the case of flow acceleration in a second-stage with long electrode rails. The second series utilized short electrodes to achieve higher mass flow rates by ablation, and a third series shortened the electrodes further to concentrate current flow near the inlet. In all tests, an actual PPT from the Lincoln Laboratories production[2] for the LES-8/9 mission was used to inject plasma between electrodes connected to a charged pulse-forming network (PFN). The PFN is a 5-section voltage-fed synthetic transmission line with a 0.75 ohm characteristic impedance. The total stored energy is 22.5 kJ with the capacitors charged to 20 kV. The output pulse risetime (and decay time) is 8% of the design pulsewidth of 185 μsec. At maximum operating voltage, the short circuit output current is 27 kA. A series ignitron switch is included in order to isolate the PFN from the experimental apparatus until the PPT plasma is ready to enter the second-stage; (this switch is for experimental convenience). In the present experiments, a series resistance of 0.75 Ω was included to prevent current reversal in the second stage.

The PPT and second-stage are stationed inside a 0.6 x 6 meter tubular stainless steel vacuum vessel that is evacuated to 10^{-6} torr prior to thruster operation. In the vicinity of the thruster, the vessel is lined with Mylar. Several ports are available for probe feedthrough and optical diagnostic access. Figure 5 provides a sketch of the basic apparatus. The geometries of the second-stage systems are shown in Figures 6 and 7, long-rail and short-rail, respectively. The inlet-rail geometry is the same as the short rail system except that the electrodes are cut back to the inlet region and Pyrex sidewalls prevent the lateral expansion of flow in the thruster.

Long Rail Experiments

The long rail second-stage consisted of a brass anode and cathode each 6 mm thick. The anode was 28 cm long, the cathode was 23 cm long and the anode-cathode separation was 8.7 cm. All electrode edges were rounded with a 3 mm radius to reduce field enhancement. The effective

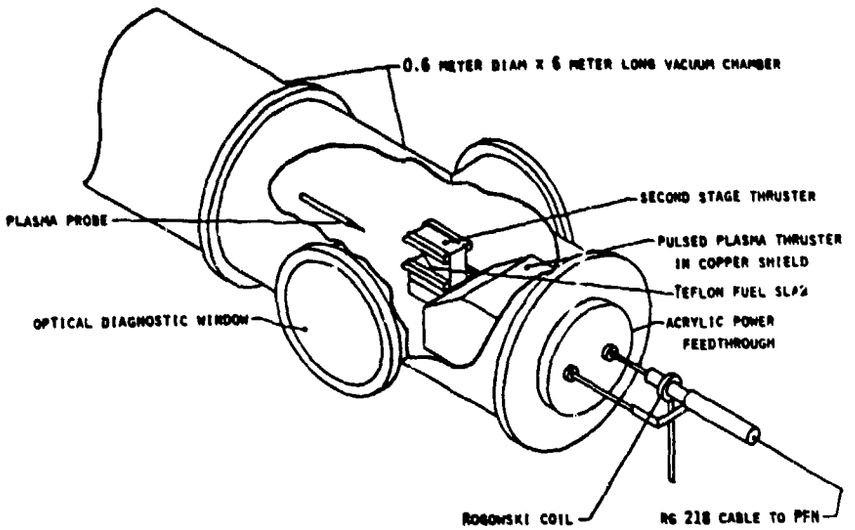

Fig 5 - Sectional view of Experimental Thruster Facility at the RDA Washington Research Laboratory.

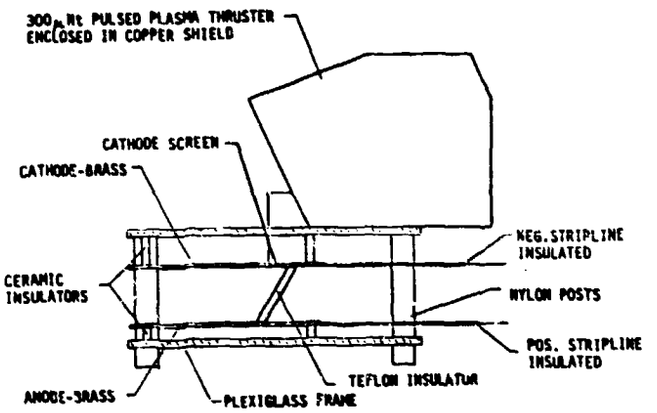

Fig 6 - Schematic diagram of long-rail experimental set-up.

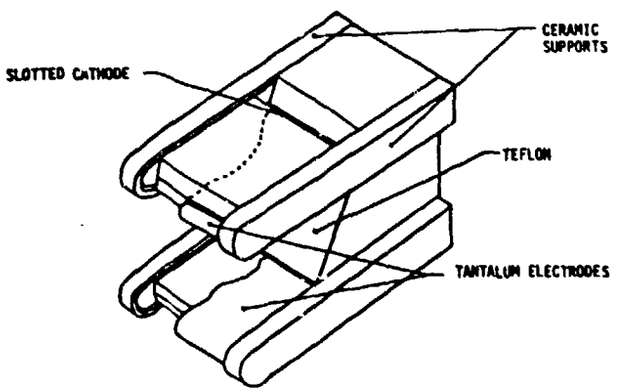

Fig 7 - Sectional view of second-stage in Short Rail Experiments. See Fig 5 for overall layout.

width of the anode and cathode was 3.5 cm. This was maintained by two vertical acrylic dielectric channel walls that extended to the ends of the electrode system. Slots 1.5 mm wide cut into the upstream end of the cathode allowed plasma from the PPT to pass through the cathode and cross the face of a 6 mm thick Teflon insulator. The Teflon insulator was inclined at an angle of 45° with respect to the central axis of the electode system. Plasma from the PPT was directed through a copper channel to the entry slots in the top of the cathode surface. A matrix of holes through the cathode beginning at 8 cm from the cathode-Teflon junction provided entry ports for magnetic B-probes into the plasma channel. Both anode and cathode rails were secured to acrylic sheet 1.27 cm thick by means of ceramic standoff insulators. The upper and lower acrylic sheets were in turn secured to each other by means of nylon rod insulators. Electrical connection to the anode and cathode was provided by braided copper straps covered with Tygon tubing. The tubing provided an insulating cover that prevented electrical breakdown between the vacuum chamber wall and the anode, and between anode and cathode.

Magnetic probes were constructed using 40 turns of #38 insulated copper wire wound on a 1 mm diameter mandrel. The coil leads were tightly twisted. The coil was then removed from the mandrel and impregnated with polystyrene. The coil was then cemented to an acrylic rod to insure constant orientation. The coil-tipped rod was then inserted into a 3 mm OD Pyrex sleeve, sealed at one end. The axis of the field-sensing coil is perpendicular to the axis of the Pyrex sleeve. For calibration, the rail gun was shorted at the muzzle end and the time resolved response of each probe was recorded along with the output of the capacitor bank/pulse-forming line. In this way a matrix of in situ calibration factors was obtained for various probe locations. The short was removed and a set of time-resolved probe responses was obtained between 10 and 16 cm downstream from the inlet to the second-stage for probe channel penetrations of 1, 2, and 3 cm.

As the discharge current rose in the second-stage, after injection of the PPT plasma, magnetic field was detected rapidly at successive downstream locations of the magnetic probes. The plasma speed, indicated by time-of-arrival of signals at the probes, is approximately 4×10^4 m/s. At 16 μsec into the current pulse pulse, over 80% of the total current is carried more than 15 cm downstream of the plasma inlet. At later times, however, this percentage drops to 70% (t=96 μsec) and 50% (t=156 μsec) indicating shunting of the current at positions closer to the inlet and second-stage Teflon insulator. Since interferometric measurements indicate that the PPT plasma pulse should be complete after about 20 μsec, the gradual shifting of current upstream may be ascribed to ablation of the Teflon insulator. With the long-rail electrode system used in these tests, it therefore appears that the PPT plasma is rapidly swept downstream resulting initially in rather low current density near the second-stage insulator. Continued heating, however, gradually creates enough mass flow to shunt current, (but by this time the current pulse in the present experiments is nearly over). Time-resolved spectroscopy indicates that Hα intensity drops off more rapidly (after the first 20 μsec of operation) than In I intensity, suggesting that electrode erosion may provide plasma for current conduction before sufficient ablation of the Teflon insulator occurs. (The Hα may be due to the surface contaminants blown out by operation with the initial PPT plasma). To achieve faster ablation of the second-stage insulator, a second series of experiments was performed with shorter electrode rails.

Short Rail Experiments

The anode and cathode of the short rail second-stage were constructed from 0.9 mm thick tantalum sheet. Each electrode was 4 cm wide with the downstream end formed into a 6 mm diameter cylinder to reduce field enhancement. Field enhancement from the sides of the electrodes was reduced by burying the metal edges in ceramic support rails to a depth of 3 mm. The rail supports maintained the 4.6 cm anode-cathode electrode separation. A solid Teflon rod 5 cm square with one end face cut at 45° with respect to the central axis of the bar was located between the electrodes. The exposed (flat) lengths of the anode and cathode were 3 cm and 8 cm respectively. Slots 3 mm wide in the cathode electrode just above the Teflon rod provided entry ports for plasma from the PPT. Plasma reached these slots by passing through a conical chute in a Teflon block that secured the short rail second-stage to the PPT. Electrical connection to the second-stage electrodes was provided by braided copper conductors. Teflon tubing 6 mm in diameter slipped over the conductors prevented plasma discharges between the experiment chamber and the braided copper anode lead and between anode and cathode leads.

The goal of the short rail two-stage thruster experiments was higher thrust at approximately the same specific impulse as the PPT by means of additional mass ablation at the second stage insulator surface. The PPT was operated at 1875 V with a stored energy/shot of 30 J. As reported previously, this device ablates approximately 30 μg/shot of Teflon (CF_2) with a specific impulse of 1100 sec and

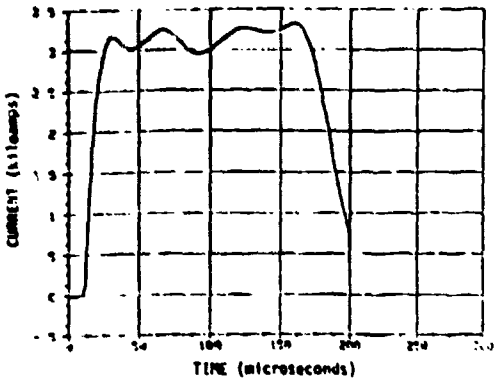

Fig 8 - Current vs time for the Short Rail Experiments with 5 kV on Pulse Forming Network.

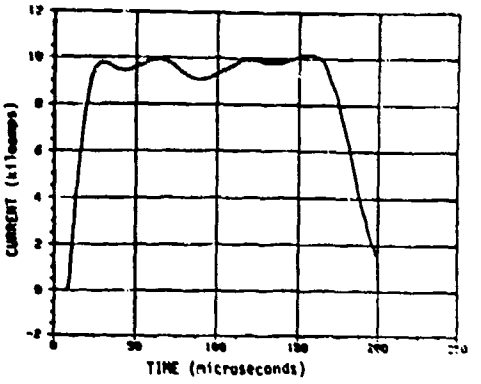

Fig 11a - Current vs Time for the Inlet-Rail Experiments with V_o =15 kV.

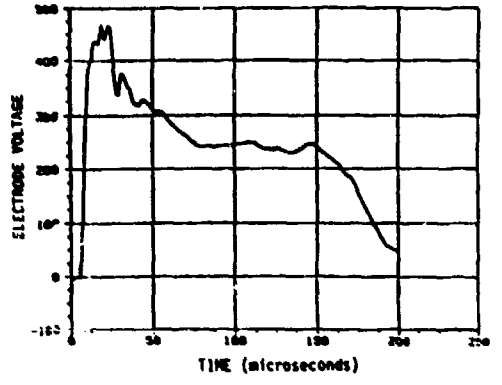

Fig 9 - Electrode Voltage vs Time for the Short Rail Experiments with V_o = 5 kV initial voltage on PFN.

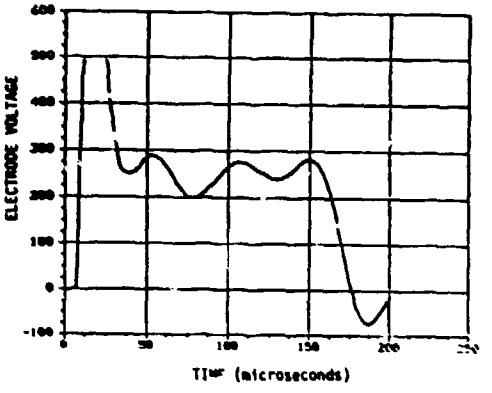

Fig 11b - Electrode Voltage vs Time for the Inlet-rail Experiments with V_o =15 kV.

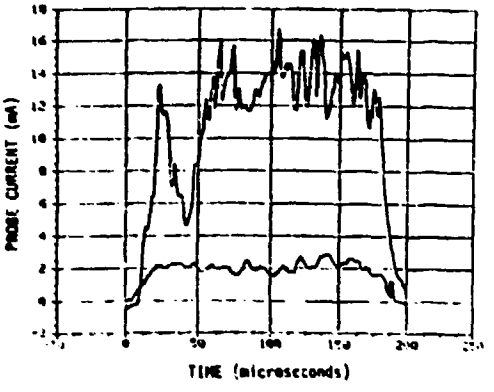

Fig 10 - Langmuir Probe Ion Saturation Current vs Time for the Short Rail Experiments V_o = 5 kV. Upper Trace Probe 13 cm from Exit, Lower Trace 33 cm from Exit.

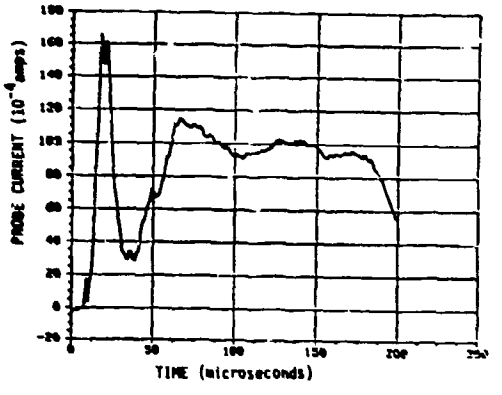

Fig 12 - Langmuir Probe Ion Saturation Current vs Time 40 cm from Exit with V_o =15 kV.

an average impulse bit of 300 μnt-sec.[3] Other work also indicates ion exit velocities of 2.8 cm/ sec and an exit plasma ionization level of 20-40%.[4]

The second stage was operated with a 5 kV charge on the PFN. Figure 8 shows a typical current trace and Figure 9 a typical voltage trace. The current risetime is 15 μsec to 3-3.25 kA. The plate voltage rises initially to about 450 kV and then falls to about 250 V in approximately 50 μsec. Integration of the product of current and voltage indicates that the total energy leposited in the second stage after the PPT transient (t>40 μsec) was about 110 J.

In order to diagnose the short rail performance, two Langmuir probes were inserted 13 and 33 cm downstream of the end of the electrodes. The probes were made of tungsten wire 0.127 mm diameter and 1 mm long held in a sealed Pyrex tube. If the probe bias is sufficiently more negative than the floating potential (measured to be V_f = +35V with second-stage cathode grounded to the vacuum tank) the ion current is saturated at a level given (for T_i=T_e) by[5]

$$I_{ion,sat} = S_p e n_e \left(\frac{kT_e}{2\pi M}\right)^{\frac{1}{2}}$$

where S_p = probe area
n_e = electron density
T_e = electron temperature
M = mass of the ions

With the two probes operating in ion current saturation, identifiable probe signatures during the middle and latter portions of the current pulse indicate a quasi-steady plasma stream velocity, u_s, of 1.7-2.5 x 10^4 m/s. Figure 10 shows typical ion saturation currents for the two probes. The observed currents are continuous and relatively constant for the duration of the discharge indicating a constant ablation and acceleration of material out of the second stage.

The directed ion velocity (plasma stream velocity) may be on the order of the ion thermal speed which would imply that the ion current collected at the probe is strongly dependent upon the probe orientation in the plasma stream. To estimate the charged particle density, we therefore use the electron saturation current. If the probe bias is higher than the plasma space potential, V_s, the electron current collected is saturated and given by[5]

$$I_{e,sat} = S_p e n_e \left(\frac{kT_e}{2\pi m_e}\right)^{\frac{1}{2}}$$

where m_e = mass of electron. Preliminary measurements of the electron temperature, T_e, of 2-8 eV imply an electron density at probe 1 of 1.4-2.9 x 10^{13} e/cm^3 and at probe 2 of 3.5-7 x 10^{12} e/cm^3. (Previous measurement of the exit plasma temperature from the PPT, assuming T_e=T_i, indicated 7.2 eV[4]).

The total mass of material ejected by the second stage can be approximated by assuming T_e and the degree of ionization α are constant at the probe positions. The lower current at the probe further downstream would then be due simply to expansion of the flow (i.e., thermal and angular spread of the exhaust jet). If a linear expansion is assumed from the exit plane of the second-stage, then the half-angle of the exhaust divergence is approximately 16°. (For Teflon, M = 16.7AMU, this divergence would correspond to a "thermal" energy of about 7 eV). The total mass flowing through the 18.4 cm^2 exit plane of the second-stage is then estimated to be 50-72 μg, assuming T_e = 7 eV, α = 30%, and u = 1.7-2.5 10^4 m/s. For the assumed speed, the impulse bit is therefore I = 0.85-1.8 x 10^{-3} nt-sec, and the kinetic energy divided by input electrical energy is 6.6-20.5%.

It should be noted that the estimated impulse implies a driving pressure of about 2.9-6.1 x 10^3 Pa, while the magnetic pressure in the second-stage should be about 1-2 x10^5 Pa. The energy for the flow may thus have substantial electrothermal contributions. In the present experiments, insulating channel walls on each side of the Teflon insulator were not used in order to force ablation only of the Teflon. The electrically-heated plasma may therefore be able to expand laterally as well as axially downstream. The total mass ablated per shot could then be up to three times larger than estimated from the Langmuir probe data. If the total mass flow could be channeled downstream by sidewalls (as in the PPT), then the kinetic efficiency of the second-stage might exceed 60%, with a total impulse in excess of 5.4 x 10^{-3} nt-sec.

Inlet-Rail Experiments

In the third series of tests, the lengths of the electrodes of the short rail system were decreased to 0.5 cm for the anode and 1.3 cm for the cathode (which has the inlet screen for the PPT plasma). The second-stage channel dimensions were maintained by substituting Teflon in the area formerly occupied by the electrodes; also, sidewalls of Pyrex were added to eliminate any lateral expansion of the plasma. The net effect of these changes is to concentrate the plasma and current density near the second-stage insulator and thereby to enhance ablation. Figure 11 displays the voltage and current record for a discharge with the PFN charged initially to V_o = 35 kV. The voltage trace is similar

to the lower energy (V_o = 5 kV) test, but the current is now about 9.5 kA. Ion saturation current, measured 40 cm downstream of the thruster exit, is shown as a function of time for the same shot in Figure 12. Tests at lower initial voltage (V_o = 5 kV, 7 kV) indicate that the ion saturation current scales as the PFN energy, suggesting that the energy per particle is remaining constant, (which would be expected for processes involving ablation and ionization). At lower system energy, it was possible to obtain the full probe characteristic and thereby estimate the plasma temperature (and also obtain a density measurement that is less sensitive to flow direction). From the slope of the probe current between floating and plasma potential, the temperature appears to be about 7 eV; the difference between floating and plasma potentials for the Teflon plasma indicates the same value. The divergence of the exhaust is also consistent with an ion temperature of 7eV. It appears then that plasma conditions are very similar to both the previous short rail tests and the earlier microthruster experiments by other groups. The difference in the present experimental series is the use of a current pulse that is maintained longer and at a constant level by means of a PFN.

For the inlet-rail tests, at the highest initial V_o, the plasma density at the exit is estimated to be n_e = 1.3 x 10^{15} e/cm^3, which would imply an ablated mass of 500-730 μg, if an ionization level α = 0.3 and flow speeds of 1.7-2.5 x 10^4 m/s are again assumed. The efficiency of conversion of input electrical energy to flow kinetic energy would thus range from 23-72% depending on the values of α and flow speed. Note that flow kinetic energy estimated using the charged particle density from probe data depends on the cube of the flow speed. Much better data are need to obtain an accurate measure of thruster performance.

Concluding Remarks

The principal result suggested by the data from the short-rail and inlet-rail experiments is that a high temperature ablation arc can be maintained on a Teflon surface for the duration of the current pulse. This arc provides a high speed plasma flow that achieves quasi-steady conditions (during the 150 μsec pulse of the present experiments, at least) with a specific impulse in the range of 2000 sec. The voltage drop across the second-stage (~200 V) is significantly larger than the cathode fall (~35 V), so the ablation arc should be rather efficient in converting electrical energy to flow energy.

Since the impulse per shot is proportional to the duration of the current pulse, there should be considerable flexibility in matching a second-stage thruster (triggered by a PPT) to a variety of mission requirements and power supply limitations. For low power missions, such as station-keeping, the multi stage system should perform like present microthrusters that have already seen application in space, but the multi stage devices can have higher thrust. As higher levels of space prime-power become available, the current pulse duration can be extended to match the available power at the same repetition rate with the same type of capacitor components used in the present PPT (so lifetime and specific power of the pulsed source should not be a problem). If still higher powers are available, higher current operation would allow magnetoplasmadynamic processes to become more important, so the second-stage could become a quasi-steady MPD arcjet (without propellant valves); alternatively, steady MPD or thermal arcjet operation would be possible. In all cases, end feeding of propellant bars, as in the PPT, allows the geometry to be preserved during longterm operation. The present preliminary work on multistage plasma propulsion thus indicates that a single thruster arrangement could be coupled to progressively higher powers simply by adjusting a single extensive variable (the pulsewidth), maintaining the basic physical processes of the thruster as space experience is accumulated.

References

1. P.J. Turchi, "An Electric Propulsion Development Strategy Based on the Pulsed Plasma Microthruster", 16th Electric Propulsion Conference, New Orleans, LA, 1982. AIAA Pre-print 82-1901.

2. R.J. Vondra, and K.I. Thomassen, "Flight Qualified Pulsed Electric Thruster for Satellite Control", Journal of Spacecraft and Rockets, Vol 11, No. 9, Sep 1974, pp. 613-617.

3. K.I. Thomassen, and R.J. Vondra, "Exhaust Velocity Studies of a Solid Teflon Pulsed Plasma Thruster", Journal of Spacecraft and Rockets, Vol 9, No. 1, Jan 1972, pp. 61-64.

4. K.I. Thomassen, and D. Tong, "Interferometric Density Measurements in the Arc of a Pulsed Plasma Thruster", Journal of Spacecraft and Rockets, Vol 10, No. 3, Mar 1973, pp. 163-164.

5. R.L. Huddlestone, and S.L. Leonard, Plasma Diagnostic Techniques, Academic Press, New York, 1965.